

Model-Based Calibration of Filter Imperfections in the Random Demodulator for Compressive Sensing

Pawel J. Pankiewicz, Thomas Arildsen, *Member, IEEE*, and Torben Larsen, *Senior Member, IEEE*

Abstract—The random demodulator is a recent compressive sensing architecture providing efficient sub-Nyquist sampling of sparse band-limited signals. The compressive sensing paradigm requires an accurate model of the analog front-end to enable correct signal reconstruction in the digital domain. In practice, hardware devices such as filters deviate from their desired design behavior due to component variations. Existing reconstruction algorithms are sensitive to such deviations, which fall into the more general category of measurement matrix perturbations. This paper proposes a model-based technique that aims to calibrate filter model mismatches to facilitate improved signal reconstruction quality. The mismatch is considered to be an additive error in the discretized impulse response. We identify the error by sampling a known calibrating signal, enabling least-squares estimation of the impulse response error. The error estimate and the known system model are used to calibrate the measurement matrix. Numerical analysis demonstrates the effectiveness of the calibration method even for highly deviating low-pass filter responses. The proposed method performance is also compared to a state of the art method based on discrete Fourier transform trigonometric interpolation.

Index Terms—Analog-digital conversion, Calibration, Compressed sensing, Error compensation, Filtering, Signal reconstruction,

I. INTRODUCTION

THE compressive sensing (CS) paradigm [1]–[3] has inspired researchers to apply the theory in practical analog signal acquisition [4]–[10]. An analog-to-digital converter (ADC) utilizing the CS framework can sample sparse or compressible signals at significantly lower frequencies than the Shannon-Nyquist theory for general and potentially dense signals dictates [11], [12]. The Shannon-Nyquist condition is a sufficient sampling criterion when no prior information on the signal composition is available. Following the principles of CS, the under-sampled signal can be reconstructed if it is sparse or compressible. Signal sparsity is modeled by expressing the signal as the linear combination of a few elements from a particular dictionary [1]. The trade-off in CS is a more complex signal recovery as it requires non-linear reconstruction algorithms [13].

The random demodulator (RD) sampling architecture has been widely explored since the introduction of the compressive sensing theory [4], [5], [8], [14]. The architecture is dedicated to the sampling of frequency-, time-frequency- or time-sparse signals [4], [10], [15] which makes it more flexible than other

analog CS architectures such as [6], [7], [9]. The acquisition process leads to fewer samples than the traditional Shannon-Nyquist method.

The RD architecture illustrated in Fig. 1, can be implemented by standard off-the-shelf components [4], [14]. The RD architecture aim is to compress an analog input signal into a smaller bandwidth, which can be further sub-sampled, encoding the signal information on smaller set of samples. The core idea behind the compression in the RD architecture is to modulate the input signal by a fast-varying chipping sequence and to low-pass filter it. The sub-sampling operation is realized by a low-rate sampling ADC. These functional procedures are modeled by the so-called measurement matrix in CS signal reconstruction algorithms [10], [14]. The reconstruction relies on the accuracy of the measurement matrix [16].

In reality, due to factors such as supply voltage, manufacturing process, temperature variations etc., the analog components do not behave ideally and hence the actual front-end differs from its ideal model. Due to the relatively low clock rate of the RD some imperfections such as clock jitter and nonlinear distortion can be neglected [14]. However, stationary imperfections such as component impairments cannot be neglected [17]. Previous studies show that generic CS reconstruction algorithms are sensitive to mismatches between the ideal and the actual analog front-end, represented by the measurement matrix [17], [18]. The need for measurement matrix calibration has therefore been emphasized in [8], [14].

An obvious solution, although impractical, is to measure the actual impulse response of each device and revise the model (measurement matrix) accordingly [8]. Existing literature also investigates the question of how much error the mismatch in the measurement matrix contributes to the reconstruction quality [19]–[21]. This is, however, an analysis of the problem – not an attempt to mitigate it. Several proposals of a more robust reconstruction have also been made [22]–[25]. The algorithms consider an additive error in the measurement matrix or dictionary. This enables a more robust signal estimate, assuming only statistical knowledge of the error.

In [10], the author discusses calibration of an analog CS architecture based on the RD. The methodology considered building the system's measurement matrix via the Fourier domain by sampling specially dedicated signal sequences. The technique is known as discrete Fourier transform trigonometric interpolation (DFTTI) [10]. The method is accurate and does not require an initial front-end model, although depending on the systems' parameters, the DFTTI might be time-consuming. The operation requires calibrating samples of the same order as the CS measurement matrix problem size $M \times N$ ($M < N$), where M denotes compressed samples and N the amount

The authors are with Aalborg University, Faculty of Engineering and Science, Department of Electronic Systems, DK-9220 Aalborg, Denmark. The authors' e-mails are: {pjp, tha, tl}@es.aau.dk. This work was financed by The Danish Council for Strategic Research under grant number 09-067056. The authors would like to thank Danish Center for Scientific Computing (DCSC) for funding.

of Nyquist samples of the input signal. Also, a blind sparse calibration of an initially modeled measurement matrix has been proposed [18]. The method calibrates the measurement matrix through M samples from U unknown (but sparse) training sequences. The procedure requires $U \times M$ calibrating measurements, where $U \ll M$.

This article proposes a supervised model-based calibration method that minimizes the discrepancy between the initially modeled measurement matrix and the actual front-end. The method exploits the nature of the error associated with the measurement matrix through sampling of an a-priori known signal to identify the errors through linear estimation. The error estimate is further used to calibrate the initially modeled measurement matrix. The method can be seen as a trade-off between the sample-expensive DFTTI supervised method and sample-efficient unsupervised sparse calibration. The successful model-based calibration requires only S supervised measurements, where $S \leq M$. In this paper we focus on the practical aspects of the RD architecture, testing the calibration on modeled component impairments. Performed signal reconstruction benchmarks with the DFTTI method [10] show significant time advantages in favor of our proposed method.

The rest of the paper is structured as follows: Section II presents the RD and CS frameworks. Section III describes the measurement matrix structure and the modeling error. Section IV presents the proposed calibration principle. Section V describes simulation framework, the case study of a passive filter with imperfect components used in the random demodulator, and calibration benchmark results. Finally, section VI presents the conclusion.

II. BACKGROUND

The RD obtains measurements \mathbf{y} according to the CS principle [4], [14]:

$$\mathbf{y} = \Phi \mathbf{x}, \quad (1)$$

where $\Phi \in \mathbb{R}^{M \times N}$, $M < N$ is the measurement matrix that represents the analog front-end of the random demodulator, $\mathbf{x} \in \mathbb{R}^{N \times 1}$ is the original signal, and $\mathbf{y} \in \mathbb{R}^{M \times 1}$ denotes compressed measurements acquired for time $t \in [0, T]$. T denotes the observation time length. The sampling rate $f_s = M/T$ needed for successful signal recovery is dictated by a lower bound of $M \geq CK \log_{10}(\frac{2B}{K} + 1)$, rather than $2B$, where B is the bandwidth of a signal, K is the signal sparsity, C is a positive constant acquired empirically [4], [14], [16]. A sparse representation is one of the necessary requirements to utilize CS [1], [2]. A model of a sparse signal can be represented as:

$$\mathbf{x} = \Psi \boldsymbol{\alpha}, \quad (2)$$

where Ψ is an $N \times N$ dictionary matrix, and $\boldsymbol{\alpha}$ of size $N \times 1$ is the underlying sparse vector, i.e., $\boldsymbol{\alpha}$ contains $K \ll N$ non-zero coefficients. Alternatively, $\boldsymbol{\alpha}$ may be compressible instead. This more relaxed requirement is met when the entries of $\boldsymbol{\alpha}$ decay rapidly to zero when sorted by magnitude.

The RD architecture is illustrated in Fig. 1. First the analog signal $x(t)$ is spread in frequency by the multiplier and $p(t)$,

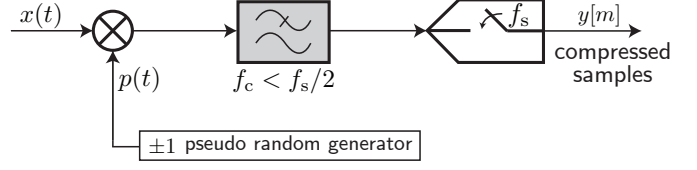


Fig. 1. Single stage random demodulator excluding quantization of the compressed measurements [4].

the signal is low-pass filtered and subsequently uniformly sampled at frequency f_s .

The compressed measurements $y[0], \dots, y[M-1]$ are then used to reconstruct the sub-sampled signal by a suitable algorithm, [1], [5], [14], [26]–[28]. The principle is to utilize the compressed measurements \mathbf{y} together with a sparsifying dictionary Ψ and measurement matrix Φ to recover the sampled signal \mathbf{x} as illustrated in Fig. 2.

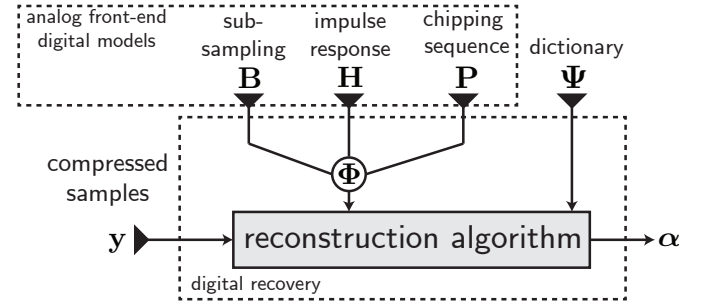


Fig. 2. Conceptual illustration of the CS signal reconstruction for the RD technique.

A. Reconstruction stage

Initially, in order to recover a sampled signal \mathbf{x} from compressed measurements \mathbf{y} , we would use the assumption of sparsity [1]. The problem in a computationally tractable form can be posed as a convex problem, where a sparse vector is recovered as: $\arg\min \|\boldsymbol{\alpha}\|_1$ s.t. $\mathbf{y} = \Phi \Psi \boldsymbol{\alpha}$.

This approach is called Basis Pursuit [29] and it belongs to the family of convex optimization methods used to recover signals within the CS framework [2].

More practical reconstruction methods can be constructed under the assumption of noise added to the compressed samples \mathbf{y} as a consequence of the sampling process, e.g., quantization in the ADC. This approach is known as Basis Pursuit De-Noising (BPDN) [29]:

$$\begin{aligned} & \underset{\boldsymbol{\alpha} \in \mathbb{C}^{N \times 1}}{\text{minimize}} && \|\boldsymbol{\alpha}\|_1 \\ & \text{subject to} && \|\mathbf{y} - \Phi \Psi \boldsymbol{\alpha}\|_2 \leq \zeta, \end{aligned} \quad (3)$$

where ζ controls the fidelity term.

The ℓ_1 -minimization techniques present strong recovery guarantees but suffer from high implementation complexity [27]. Apart from convex optimization approaches, there is a group of methods called greedy algorithms where the unknown support of the signal is calculated iteratively. The Orthogonal Matching Pursuit (OMP) [27] and the Subspace Pursuit (SP) [28] are some of the most popular methods in this group.

B. Functionality of the acquisition stage

The RD architecture is dedicated to handling band-limited signals and assumes that the analog signal $x(t)$ is composed of a discrete, finite number of weighted continuous dictionary components as [4], [5]:

$$x(t) = \sum_{n=0}^{N-1} \alpha_n \psi_n(t), \quad t \in [0, T], \quad (4)$$

where, e.g., $\alpha_0, \dots, \alpha_{N-1} \in \mathbb{C}$ for frequency-sparse signals could represent Fourier series coefficients $\psi_n(t) = \exp[-j2\pi nt]$ [14].

The RD signal acquisition starts with a spread spectrum operation. The operation is carried out by multiplying the input signal by the chipping sequence, produced by a random number generator:

$$d(t) = x(t) p(t), \quad (5)$$

where $p(t)$ is the chipping sequence. The zero-mean ± 1 chipping sequence has to be alternating at the frequency $f_{\text{chip}} > 2B$ of the input signal [10], [14]. According to [10], it is desirable that f_{chip} is as close as possible to the lower bound to keep most of the power in-band.

The filtering operation can be represented as a convolution of the mixed signal with the impulse response of the filter h [5]:

$$x_{\text{lpf}}(t) = \int_{-\infty}^{+\infty} d(\tau) h(t - \tau) d\tau. \quad (6)$$

Lastly, the filtered signal x_{lpf} is uniformly sampled at the rate f_s and yields compressed measurements $\mathbf{y} \in \mathbb{R}^{M \times 1}$.

The system described by (5)–(6) and the sampling are linear operations. Considering the signal model in (4), the discrete compressed measurement vector can be characterized as a linear transformation of the discrete coefficient vector $\boldsymbol{\alpha}$. Further expanding (6), as shown in [4], results in the following model for the compressed measurements discrete vector:

$$y[m] = \sum_{n=0}^{N-1} \alpha_n \int_{-\infty}^{+\infty} \psi_n(\tau) p(\tau) h(mf_s^{-1} - \tau) d\tau. \quad (7)$$

The model of the analog front-end in the reconstruction stage is represented in a digital form and (7) is therefore discretized to the following form¹:

$$y[m] \simeq \sum_{v=0}^{N-1} \sum_{n=0}^{N-1} \alpha[v] \psi[v, n] p[n] h[mR - n], \quad (8)$$

and by utilizing the sparse model in (2):

$$\mathbf{y}[m] \simeq \sum_{n=0}^{N-1} x[n] p[n] h[mR - n], \quad (9)$$

where $R = f_{2B}/f_s = N/M \in \mathbb{N}^1$ is a positive integer that defines the sub-sampling ratio in discretized form [16]. The operations on the right hand side of (8) are expressed using a linear transformation $\mathbf{y} = \mathbf{\Phi} \mathbf{\Psi} \boldsymbol{\alpha}$. The dictionary and filter matrices entail both time and frequency discretization of the

dictionary and time discretization of the filter. As described in the introduction section, $\mathbf{\Phi}$ is the measurement matrix mapping \mathbf{x} to the compressed set of measurements \mathbf{y} , and $\mathbf{\Psi}$ is the sparsity basis with assumption of integer tone separation equal to 1, in the case of frequency sparse signals [14], [16].

III. MEASUREMENT MATRIX STRUCTURE

The measurement matrix represents a model of the operations undergone by the signal during acquisition [15]. From (7) and (9) we can isolate expressions for modulation, filtering and sampling:

$$\mathbf{\Phi} = \mathbf{B} \mathbf{H} \mathbf{P}, \quad (10)$$

where the matrix $\mathbf{\Phi}$ is considered the product of three matrix factors representing the uniform sub-sampling $\mathbf{B} \in \mathbb{Z}^{M \times N}$, impulse response of the filter $\mathbf{H} \in \mathbb{R}^{N \times N}$ and chipping sequence $\mathbf{P} \in \mathbb{Z}^{N \times N}$.

The chipping sequence matrix is defined as follows:

$$\mathbf{P} = \text{diag}(p[0], p[1], \dots, p[N-1]) \in \{\pm 1\}^{N \times N}, \quad (11)$$

The spread spectrum operation in (5), in the discrete form, is interpreted as a product of \mathbf{x} and \mathbf{P} , that yields N demodulated samples:

$$d[n] = x[n] p[n], \quad n \in \{0, \dots, N-1\}. \quad (12)$$

The matrix representing an approximation of the infinite impulse response of the filter or more generally linear time invariant (LTI) system has the form of a banded N -by- N Toeplitz matrix:

$$\mathbf{H} = \begin{bmatrix} h[0] & h[-1] & h[-2] & \dots & \dots & h[-N+1] \\ h[1] & h[0] & h[-1] & \ddots & & \vdots \\ h[2] & h[1] & \ddots & \ddots & \ddots & \vdots \\ \vdots & \ddots & \ddots & \ddots & h[-1] & h[-2] \\ \vdots & & \ddots & h[1] & h[0] & h[-1] \\ h[N-1] & \dots & \dots & h[2] & h[1] & h[0] \end{bmatrix}, \quad (13)$$

where $\mathbf{h} = [h[0], \dots, h[L-2], h[L-1]]^T \in \mathbb{R}^{L \times 1}$ represents $L \leq N$ consecutive impulse response samples. For simplicity we assume causal LTI and finite impulse approximation $h[l] = 0$ for $l > L-1 \vee l < 0$ in this paper.

The sub-sampling matrix \mathbf{B} is a wide matrix that characterizes the sampling scheme:

$$\mathbf{B} = \bigoplus_{m=1}^M \boldsymbol{\kappa}, \quad \in \{0, 1\}^{M \times N}, \quad (14)$$

where $\boldsymbol{\kappa} \in \{0, 1\}^{1 \times R}$ such that:

$$\kappa[n] = \begin{cases} 1, & \text{for } n = 1 \\ 0, & \text{otherwise} \end{cases},$$

and \bigoplus denotes direct matrix sum. This matrix can be seen as containing a subset of the rows of an identity matrix, with all but each R 'th row removed.

The width of the matrices \mathbf{B} , \mathbf{H} and \mathbf{P} depends on how densely we represent the sampled signal after reconstruction. The matrix $\mathbf{\Phi}$ of width N enables reconstruction of the

¹Assuming that $x(t)$ and $p(t)$ are equal to zero for $t < 0$, and impulse response is discretized to N samples.

input signal in the Nyquist-rate resolution. Moreover, it is the minimum size, although a higher dimension may be chosen. An important factor is also the desired discrete representation accuracy of the filter's impulse response. Here it is worth noticing that this RD framework considers low-pass filters but the literature also suggests the usage of an accumulate-and-dump architecture [10], [14], [16]. In that case, an integrator with a reset system would be utilized [6], [7], [10], [14]. From the transfer function perspective, the integrator behaves similar to a low-pass filter although it does not have flat pass-band response. Discussions regarding advantages and disadvantages of using one or the other solution are not the main concern of this article and we recommend [10] for more details. The notable difference in the case of using the accumulate-and-dump architecture is that it can be easily represented in a discrete model [16]. Ideally, the integrator's impulse response is flat with unity amplitude and finite length of R . Using a low-pass filter, we deal with an infinite impulse response that needs to be approximated by the finite discrete-time model.

A. Impulse response matrix

An analog filter in the RD front-end can be described by a proper rational transfer function [30]:

$$H_a(s) = \sum_{b=0}^B \lambda_b s^b \bigg/ \sum_{b=0}^A \beta_b s^b, \quad (15)$$

where $\lambda_0, \beta_0, \dots, \lambda_A, \beta_A \in \mathbb{R}$, $B < A$, s is the Laplace s -plane variable and $H_a(s)$ is the Laplace-transform of the impulse response $h_a(t)$.

In order to build the impulse response matrix \mathbf{H} , the essential task is to obtain the discrete impulse response of the analog filter which should accurately describe the filter. Many methods exist that transform the analog transfer function to the discrete-time counterpart e.g., bilinear transform (Tustin approximation) or the impulse invariance method [31]. The methods differ in mapping accuracy, computational complexity and filter type applicability.

In cases where we deal with piecewise-constant frequency magnitude characteristics, such as lowpass, highpass and bandpass filters, the common approach is to use bilinear transformation [31]. The method essentially translates the filter transfer function (15) from the continuous-time Laplace-domain to the discrete-time z -domain by the transformation: $s \leftarrow \frac{2}{T_z} \frac{z-1}{z+1}$, where $z = \exp[j\omega T_z]$ and T_z is the sampling period.

The discrete-time transfer function is expressed as follows:

$$H_d(z) = \frac{\sum_{\ell=0}^B b_\ell z^{-\ell}}{\sum_{\ell=0}^A a_\ell z^{-\ell}} = \frac{b_0 \prod_{\ell=1}^B (1 - d_\ell z^{-1})}{a_0 \prod_{\ell=1}^A (1 - q_\ell z^{-1})}, \quad (16)$$

where d_ℓ 's are the non-zero zeros of $H_d(z)$ and the q_ℓ 's are the non-zero poles of $H_d(z)$. The discrete impulse response of the filter can be extracted through partial fraction expansion

of H_d [31]. Assuming that the poles are 1st order, the transfer function can then be expressed as partial fractions [31]:

$$H_d(z) = \sum_{\ell=1}^A \frac{U_\ell}{1 - q_\ell z^{-1}}, \quad (17)$$

where $U_\ell = (1 - q_\ell z^{-1})H_d(z)|_{z=q_\ell}$.

The inverse z -transform is then calculated as a sum of partial inverse transforms, yielding discrete-time impulse response $h[1], \dots, h[l]$.

B. Perturbed models

In CS analog acquisition, the inevitable situation, when the sampling front-end deviates from the initial model due to hardware imperfections, has been identified as measurement matrix perturbation. Furthermore, when the perturbation has a certain structure, we refer to it as structured perturbation of Φ [19]. When an additive noise in the compressed measurements is additionally included, we consider the model completely perturbed [19]. The error introduced by the sampling hardware results in an error that is correlated with the input signal $x(t)$ [22].

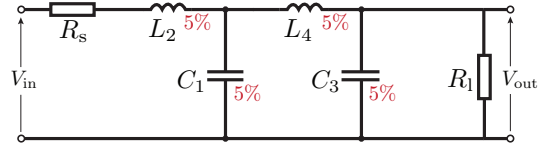


Fig. 3. Example of a low-pass filter architecture (a 4th order double-resistively terminated LC network) used in the case study.

One of the main sources of perturbation in Φ is the low-pass filter and the sensitivity of the filter transfer function to non-exact component values [17]. Depending on the filter type, components might deviate from their nominal values due to the manufacturing process (component tolerance), device mismatch [32]–[34] or parasitic components in the circuitry. These differences in component values change the shape of the implemented frequency response and cannot be controlled by the designer [35].

Fig. 4 shows the impulse responses of a double-resistively terminated LC network (Fig. 3) realization of a 4th order low-pass Butterworth filter where the components differ up to 5% from their nominal values according to a truncated (5% of the mean) Gaussian distribution.

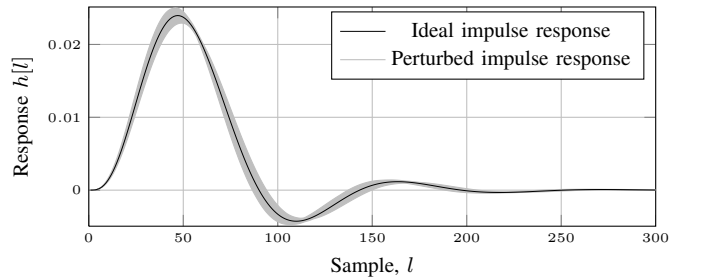


Fig. 4. Discrete impulse responses of the 4th order Butterworth low-pass filter from Fig. 3. Ideal impulse response and 1000 randomly generated perturbed impulse responses from components subject to up to $\pm 5\%$ deviations.

The error in the digital model of the impulse response can be considered additive and we can thus model the impulse response error matrix using the same structure as the \mathbf{H} matrix has:

$$\hat{\mathbf{H}} = \mathbf{H} + \mathbf{E}, \quad (18)$$

where \mathbf{H} represents the ideal impulse response matrix, $\hat{\mathbf{H}}$ is the realized impulse response matrix, and \mathbf{E} is the error matrix. The error matrix can be represented by the simplified² structured model below:

$$\mathbf{E} = \begin{bmatrix} e[0] & 0 & 0 & \dots & \dots & 0 \\ e[1] & e[0] & 0 & \ddots & & \vdots \\ e[2] & e[1] & \ddots & \ddots & \ddots & \vdots \\ \vdots & \ddots & \ddots & \ddots & 0 & 0 \\ \vdots & & & & e[1] & e[0] & 0 \\ e[N-1] & \dots & \dots & e[2] & e[1] & e[0] \end{bmatrix}, \quad (19)$$

where $\mathbf{e} = [e[0], \dots, e[L-1]]^T \in \mathbb{R}^{L \times 1}$ and $L \leq N$ represents the error vector between the actual impulse response of the system $\hat{\mathbf{h}}$ and the modeled \mathbf{h} :

$$\mathbf{e} = \hat{\mathbf{h}} - \mathbf{h}. \quad (20)$$

Previous research in [17] has shown that this kind of structured perturbation degrades the reconstructed signal quality of generic CS reconstruction algorithms. Most of the generic reconstruction algorithms can only deal with partially perturbed models $\mathbf{y} = \Phi \mathbf{x} + \mathbf{w}$, considering added noise \mathbf{w} to the measurements [36]–[38]. The reconstruction algorithms assume the nominal hardware component values represented by the discrete measurement model $\mathbf{y} = \Phi \mathbf{x}$. In practice, the hardware system performs the sampling operation $\hat{\mathbf{y}} = \hat{\Phi} \mathbf{x}$, where $\hat{\Phi} = \mathbf{B}\hat{\mathbf{H}}\mathbf{P} = \Phi + \mathbf{BEP}$. Consequently, the measurements $\hat{\mathbf{y}}$ obtained from the hardware system correspond to the ideal measurements with correlated additive noise $\hat{\mathbf{y}} = \mathbf{y} + \mathbf{BEPx}$.

IV. CALIBRATION METHODOLOGY

In the calibration scenario proposed, we exploit the structure of the perturbation \mathbf{E} to perform supervised calibration utilizing only $M_q \sim L$ samples of a known arbitrary sequence.

A. Linear estimation of the impulse response model error

In order to calibrate the existing measurement matrix, we need to estimate the error matrix \mathbf{E} . Assuming that the RD system can sample a known signal $\mathbf{x}_q \in \mathbb{R}^{S \times 1}$, $M_q < S$ (e.g. from a generator), we can exploit the fact that the structure of the error is already known:

$$\hat{\mathbf{y}}_q = \hat{\Phi} \mathbf{x}_q. \quad (21)$$

Under the assumption of known input signal \mathbf{x}_q and front-end model Φ , we can rearrange the measurement equation such that \mathbf{E} becomes the only unknown:

$$\hat{\mathbf{y}}_q = \Phi \mathbf{x}_q + \mathbf{BEPx}_q. \quad (22)$$

²The model does not consider truncation of the impulse response of the filter which in theory is infinitely long. The error matrix is simplified to reflect a causal system.

Given $\mathbf{y}_q \in \mathbb{R}^{M_q \times 1}$ and the ideal measurements $\mathbf{y}_q = \Phi \mathbf{x}_q$, the difference between the modeled low-pass filter response and the actual response can be modeled as:

$$\hat{\mathbf{y}}_q - \mathbf{y}_q = \mathbf{BEPx}_q. \quad (23)$$

Furthermore, the roles of \mathbf{E} and \mathbf{x}_q can be interchanged as follows:

$$\mathbf{BEPx}_q = \mathbf{De} \quad (24)$$

where:

$$\mathbf{D} = \begin{bmatrix} d[1] & \dots & d[L] \\ d[R+1] & \dots & d[R+L] \\ d[2R+1] & \dots & d[2R+L] \\ \vdots & & \vdots \\ d[N-L+1] & \dots & d[N] \end{bmatrix} \in \mathbb{R}^{M \times L}. \quad (25)$$

The matrix \mathbf{D} is based on (12) and L is the size of the discrete impulse response vector. When $L > R$, \mathbf{D} becomes rank deficient and should be tailored by truncating its first L/R rows and discarding the first L/R measurements of $\hat{\mathbf{y}}_q$ and \mathbf{y}_q . To avoid rounding errors, $L/R \in \mathbb{Z}$ is required.

Equation (23) can be further rewritten using (24) to the following form:

$$\mathbf{De} = \hat{\mathbf{y}}_q - \mathbf{y}_q. \quad (26)$$

If the system (26) is overdetermined ($M > L$), we can use a least-squares estimator to calculate \mathbf{e} . Due to the banded-Toeplitz structure of \mathbf{H} and \mathbf{E} , estimating \mathbf{e} from (23) consequently amounts to calibrating the entire $\hat{\Phi} = \mathbf{B}\hat{\mathbf{H}}\mathbf{P}$ matrix in the reconstruction. The process can be defined as:

$$\underset{\mathbf{e} \in \mathbb{R}^{L \times 1}}{\text{minimize}} \quad \|\mathbf{De} - \tilde{\mathbf{y}}\|_2^2, \quad (27)$$

where:

$$\tilde{\mathbf{y}} = \mathbf{y}_q - \hat{\mathbf{y}}_q. \quad (28)$$

The impulse response model error can also be estimated in cases where the number of calibration measurements $M \leq L$. In this case we could use Tikhonov-regularized least-squares defined as follows [39]:

$$\begin{aligned} &\underset{\mathbf{e} \in \mathbb{R}^{L \times 1}}{\text{minimize}} \quad \|\mathbf{De} - \tilde{\mathbf{y}}\|_2^2 \\ &\text{subject to} \quad \|\mathbf{Ge}\|_2^2 \leq \gamma, \end{aligned} \quad (29)$$

where $\gamma > 0$ is a regularization parameter determining the sensitivity of the solution and $\mathbf{G} \in \mathbb{R}^{L \times L}$ is a regularization operator. This particular problem has been posed with $\gamma = \lambda_{\min}(\mathbf{D}\mathbf{D}^T)$ and $\mathbf{G} = \text{diag}(\mathbf{g}, \mathbf{v})$, where $\mathbf{g} \in \{1\}^{L/2 \times 1}$, $\mathbf{v} \in \{0\}^{L/2 \times 1}$.

Based on (27) and (29) we propose the model-based calibration (MBC) algorithm for the RD framework presented in Algorithm 1.

Having estimated $\hat{\mathbf{e}}$, from (27) or (29), we can create a calibrated impulse response matrix $\hat{\hat{\mathbf{H}}}$ and thus an updated measurement matrix $\hat{\hat{\Phi}}$. The method enables calibration of the RD filter matrix without any additional changes in the architecture and it is compatible with arbitrary CS reconstruction algorithms. Even though the method in principle calibrates the impulse response \mathbf{h} , it can compensate for more than only filter model perturbation. The uncertainty of e.g., an amplifier gain

Algorithm 1 Model-based calibration (MBC) of the impulse response model $\hat{\mathbf{H}}$ in the random demodulation architecture.

Input: known signal $\mathbf{x}_q \in \mathbb{R}^{S \times 1}$, chipping sequence $p[1], \dots, p[N]$, number of measurements: M_q , initial impulse response size L , $\Phi \in \mathbb{R}^{M_q \times N}$.

1. $\hat{\mathbf{y}}_q \leftarrow \hat{\Phi} \mathbf{x}_q \leftarrow (21)$
2. $\mathbf{y}_q \leftarrow \Phi \mathbf{x}_q \leftarrow (1)$
3. $\tilde{\mathbf{y}} \leftarrow \mathbf{y}_q - \hat{\mathbf{y}}_q \leftarrow (28)$
4. $\mathbf{D}[1 : M, 1 : L] \leftarrow d[1], \dots, d[N] \leftarrow (12), (25)$
5. **if** $L > R$ **then**
6. $\mathbf{D} \leftarrow \mathbf{D}[\frac{L}{R} : \text{end}, :] \wedge \frac{L}{R} \in \mathbb{N}$
7. $\tilde{\mathbf{y}} \leftarrow \tilde{\mathbf{y}}[\frac{L}{R} : \text{end}, :]$
8. $M_q \leftarrow M_q - \frac{L}{R}$
9. **end if**
10. **if** $M_q \geq L$ **then**
11. calculate $\hat{\mathbf{e}}$ using (27)
12. **else**
13. calculate $\hat{\mathbf{e}}$ using (29)
14. **end if**
15. $\hat{\mathbf{h}} \leftarrow \mathbf{h} - \hat{\mathbf{e}}$
16. $\hat{\mathbf{H}} \leftarrow \hat{\mathbf{h}} \leftarrow (13)$
17. $\hat{\Phi} \leftarrow \mathbf{BHP} \leftarrow (10)$
18. **Output:** $\hat{\Phi} \in \mathbb{R}^{M \times N}$

can be calibrated, where $\hat{\mathbf{y}}_q = \hat{\Phi} \mathbf{x}_q$, as long as we deal with an uncertainty of a linear system.

V. SIMULATION FRAMEWORK

We design a set of numerical simulations to verify and evaluate the proposed calibration approaches. The simulation environment³, developed in MATLAB 2012a and executed on PC, Ubuntu 12.04 LTS–Intel X5670 2.93 GHz, is divided in two separate parts:

- 1) Modeling component deviations in the low-pass filter according to specified tolerances and evaluating RD performance under perturbed models without calibration.
- 2) Performance analysis of the calibration Algorithm 1. The analysis is based on two Monte Carlo simulation schemes. The first scheme evaluates the error between the calibrated impulse response and its original value. The second approach focuses on the BPDN reconstruction with calibrated measurement matrix.

A. Filter case study

We consider a passive low-pass filter architecture utilized by the RD front-end. One of the main drawbacks in using passive filters is their transfer function sensitivity to element (component) changes. For our experiments we have chosen the doubly resistive terminated LC ladder network designed for maximum power transfer and therefore with superior sensitivity properties. The passive architecture has been chosen here to facilitate modeling of the components variations, but the observations do apply to any discrepancy between filter model and the actual hardware.

³To reproduce the experiments – the MATLAB code is freely available at: <http://www.sparsesampling.com/mbc>

The filter in Fig. 3 can be characterized by the transfer function:

$$H_{LC}(s) = \frac{\lambda_0}{4} \sum_{c=0} \beta_c s^c, \quad (30)$$

where

$$\begin{aligned} \beta_0 &= \frac{R_s}{R_l} + 1, \quad \beta_1 = L_4 + L_2 + C_1 \frac{R_s}{R_l} + C_3 \frac{R_s}{R_l}, \\ \beta_2 &= L_4 C_1 + L_2 C_1 + L_2 C_3 \frac{R_s}{R_l} + L_4 C_3, \\ \beta_3 &= L_4 L_2 C_3 + L_2 C_3 C_1 \frac{R_s}{R_l}, \\ \beta_4 &= L_4 L_2 C_3 C_4, \quad \lambda_0 = \sqrt{\frac{4R_s}{R_l}}. \end{aligned}$$

We conduct a series of numerical experiments to evaluate the effect of filter component deviations on the CS reconstruction quality. The test strategy is divided into four scenarios. Each scenario considers deviation in one filter component $\{C_1, C_3, L_2 \text{ or } L_4\}$, affecting the filter characteristics, and therefore causing measurement matrix mismatch during the reconstruction stage. This allows us to investigate how much a single component variation can influence the reconstruction. Furthermore, we consider deviation of all components and apply the proposed calibration approach in (27) or (29) to compensate the filter imperfections and evaluate the performance. In our experiments, we have used a multi-tone signal with $K - 1$ randomly chosen tones from a tone dictionary $F \in \{2, 3, \dots, 1500\}$ Hz and an amplitude dictionary $a \in \{1, 2, \dots, 10\}$. We have used a calibrating signal \mathbf{x}_q with $K = 10$ tones and input signal \mathbf{x} for the RD reconstruction tests with $K = 5$. One tone is always set to 1500 Hz to provide consistent Nyquist frequency f_{2B} . In the reconstruction stage, the framework processes 1 s of an input signal \mathbf{x} , which is represented by $N = 12600$ samples ($f_N = 4.2 \cdot 2B$); the oversampled representation is used to emulate continuous-time analog signals. We have synthesized the low-pass filter with a 3 dB cut-off frequency $f_c = 500$ Hz as Butterworth and Chebyshev approximations with the component values listed in Table I [30].

TABLE I
4TH ORDER LC-LADDER COMPONENTS IN CONSIDERED APPROXIMATIONS
FOR $f_c = 500$ Hz.

	C_1 [μF]	C_3 [μF]	L_2 [mH]	L_4 [mH]	R_s [Ω]	R_l [Ω]
Butterworth	4.9	11.8	29.4	12.2	50.0	50.0
Chebyshev	5.8	7.9	36.1	24.6	50.0	100.0

The transfer function $H_{LC}(s)$ has been discretized using bilinear transform and a sampling frequency ($\frac{1}{T_s}$) of 13 kHz. The calculated discrete impulse response $h_{LC}[l]$ has been used to define the measurement matrix $\Phi \in \mathbb{R}^{M \times N}$. The sub-sampling frequency f_s has been set to 1.05 kHz ($2f_{\text{cut}}$). Using IDFT as dictionary $\Psi \in \mathbb{C}^{N \times N}$ in the reconstruction

algorithm enables reconstruction ($\hat{\mathbf{x}}$) of the input signals $\mathbf{x} \in \mathbb{R}^{N \times 1}$. The reconstruction quality is assessed in terms of the Signal-to-Noise Ratio (SNR) defined as:

$$\xi = 20 \log_{10} \left(\frac{\|\mathbf{x}\|_2}{\|\mathbf{x} - \hat{\mathbf{x}}\|_2} \right). \quad (31)$$

We have assumed a production line yielding components according to the following expression [40]:

$$\theta_{\mu,\sigma}(c) = \begin{cases} \frac{1}{\sigma\sqrt{2\pi}} \exp \left[-\frac{(c-\mu)^2}{2\sigma^2} \right], & \text{for } |c-\mu| \leq \sigma \\ 0, & \text{otherwise} \end{cases}. \quad (32)$$

In this article we refer to (32) as a truncated Gaussian distribution. The standard deviation σ is set to 2% of the nominal component value μ . Additional quality control with an aim of max (e.g., 2%) tolerance is modeled as a truncation of the component distribution.

In the initial experiment we have performed Monte Carlo simulations, analyzing the effect of single-component deviation. The simulations considered 1000 different component values according to (32) for considered single-component variation of L_2, L_4, C_1 , and C_4 in the Butterworth low-pass filter. Reconstruction was performed with the BPDN algorithm using the SPGL1⁴ solver [29], [41]. The results are presented in Fig. 5. Despite using the least sensitive passive filter architecture, the single-component deviation according to (32) with $\mu \in \{L_2, L_4, C_1, C_3\}$, and $\sigma = 0.02\mu$, causes the average reconstruction quality of approximately 47–54 dB as opposed to 87 dB in case of a known model. A small reconstruction variation in the known model case is caused by the change of filter characteristics due to component variation but it is relatively small compared to the unknown perturbation case.

B. Calibration performance evaluation

Algorithms 2 and 3 provide a general overview of the MBC algorithm performance analysis. Algorithm 2 describes the process of obtaining compressed samples and evaluating reconstruction performance assuming no calibration has been done.

We have tested the described 4th order LC ladder network in which all the components were subject to nominal value deviations according to (32). The distribution of $p = 3000$ has been simulated, creating 3000 different component sets: $\{L_{2,1}, L_{4,1}, C_{1,1}, C_{3,1}\} \dots \{L_{2,p}, L_{4,p}, C_{1,p}, C_{3,p}\}$. In each case we have calculated the Root Mean Square Error (RMSE) of (20) – which we denote $Q(\mathbf{e}_p)$. Further, we have performed calibration according to Algorithm 1 and calculated the RMSE values between the calibrated impulse response $\hat{\mathbf{h}}$ and the actual $\hat{\mathbf{h}}$ (deviating) impulse response:

$$Q(\hat{\mathbf{e}}_p) = \frac{1}{\sqrt{L}} \|\hat{\mathbf{h}} - \hat{\mathbf{h}}\|_2. \quad (33)$$

Two calibrating scenarios have been considered, where the first assumes taking $M \geq L$ measurements of \mathbf{x}_q and estimates the

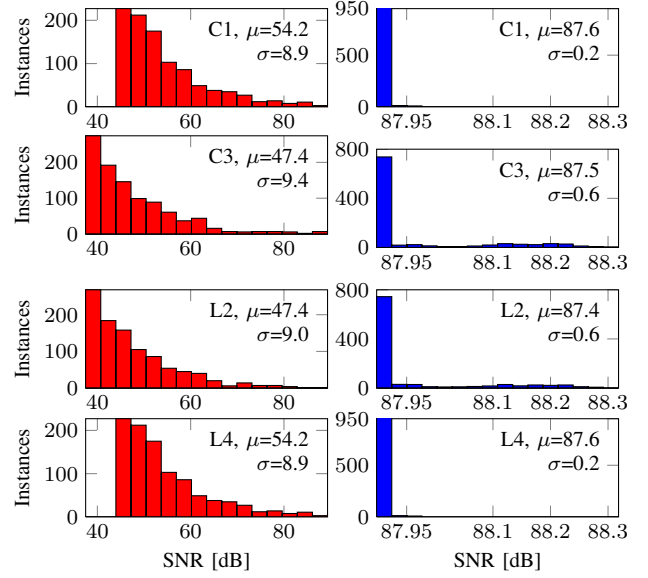


Fig. 5. Instances versus SNR bins for 1000 Monte Carlo simulations. Right column represents BPDN reconstruction quality using the measurement matrix matching every instance of deviated filter. The left column corresponds to the reconstruction quality assuming ideal filter impulse response in the model.

error in the impulse response by solving (27). The second scenario examines an undetermined system, where $M < L$. The system is calibrated by solving (29). The normalized results of the Monte Carlo simulations (with respect to iteration numbers) of $Q(\mathbf{e}_p)$ and $Q(\hat{\mathbf{e}}_p)$ are shown in Fig. 6.

Algorithm 2 RD performance under filter perturbations

Input: $\mathbf{x} \in \mathbb{R}^{N \times 1}$, component tolerances, CS measurements, sub-sampling frequency f_s , p , $f_c = \frac{f_s}{2}$, M , N

1. synthesize filter (30) $\leftarrow \mu_0 = \{L_{2,0}, L_{4,0}, C_{1,0}, C_{3,0}\}$ according to (Table I); obtain: $\mathbf{H} \in \mathbb{R}^{M \times N}$
2. generate chipping sequence $p(n)$ and the matrix in (11)
3. construct $\Phi \in \mathbb{R}^{M \times N}$ according to (10)
4. create sparsity basis IDFT matrix $\Psi \in \mathbb{C}^{N \times N}$
5. **for** $c = 1$ to p **do**
6. $\mu_c = \{L_{2,c}, L_{4,c}, C_{1,c}, C_{3,c}\} \leftarrow (32)$
7. sample $\hat{\mathbf{y}}_c = \Phi_c \mathbf{x}$ analogous to (21)
8. reconstruct $\hat{\alpha}_c \leftarrow \text{SPGL1}(\Phi, \Psi, \hat{\mathbf{y}}) \leftarrow (3)$
9. recover \mathbf{x} : $\hat{\mathbf{x}}_c = \Re\{\Psi \hat{\alpha}_c\}$, \Re denotes real-part
10. $Q(\mathbf{e}_c) = \frac{1}{\sqrt{L}} \|\mathbf{h} - \hat{\mathbf{h}}_c\|_2$
11. Compute SNR $\xi_c \leftarrow (31)$
12. **end for**
13. **Output:** Performance merits: $Q(\mathbf{e}_c)$ (RMSE), ξ_c [dB]

The mean value of $Q(\mathbf{e}_p)$ over the entire simulation for the Butterworth approximation was computed to $3.22 \cdot 10^{-4}$. After calibration (27) using $M = 189$ samples, the mean value of $Q(\hat{\mathbf{e}}_p)$ equals $3.6 \cdot 10^{-5}$, which is ≈ 9 times lower than the mean RMSE of the initial perturbation $Q(\mathbf{e}_p)$. The calibration expressed by (29) performed by taking $M = 105$ compressed samples results in mean RMSE of $1.18 \cdot 10^{-4}$, which on average is 2.7 times smaller than the mean error of the initial perturbations. The impulse response of the Chebyshev

⁴A solver for large-scale sparse reconstruction <http://www.cs.ubc.ca/labs/sci/spgl1>.

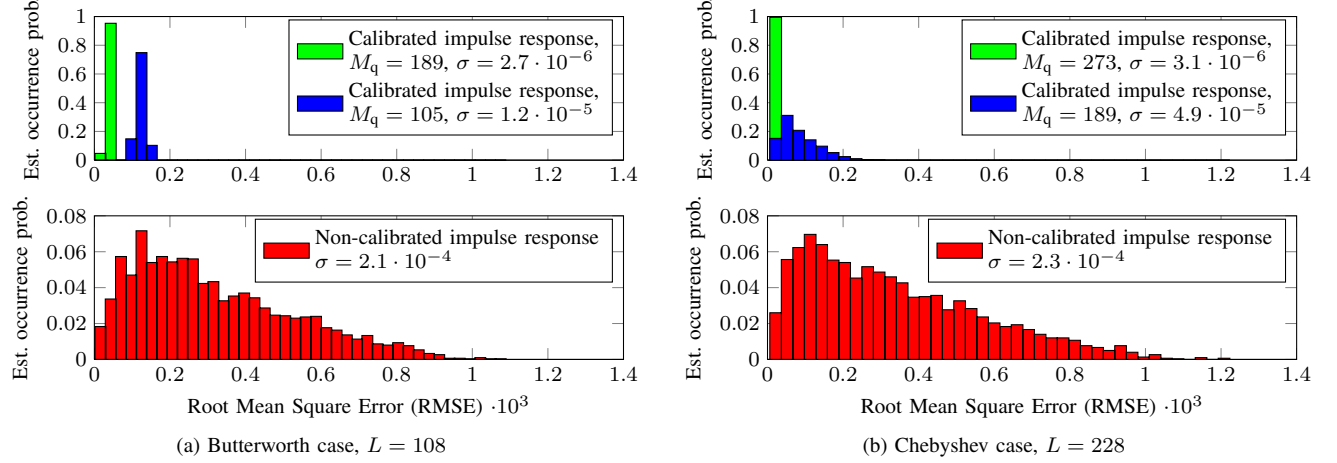


Fig. 6. Calibration performance on the random demodulator using a filter with components subject to deviations of 2 % for capacitors and inductors. Calibration methods (27) and (29) were conducted for cases $M_q > L$ and $M_q < L$ respectively.

Algorithm 3 MBC performance analysis

Input: reuse data from Algorithm 2 (\mathbf{x} , $\hat{\mathbf{y}}$, $\hat{\Phi}$, μ_c)

1. **for** $c = 1$ **to** p **do**
2. obtain $\hat{\Phi}_c$ using Algorithm 1
3. reconstruct $\hat{\alpha}_c$ (3) using SPGL1 with $\hat{\Phi}_c$, Ψ
4. recover \mathbf{x} : $\hat{\mathbf{x}}_c = \Re\{\Psi \hat{\alpha}_c\}$
5. $Q(\hat{\mathbf{e}}_c) \leftarrow (33)$
6. Compute SNR $\hat{\xi}_c \leftarrow (31)$
7. **end for**
8. **Output:** Performance vectors: $Q(\mathbf{e}_c)$ (RMSE), ξ [dB]

approximated filter was represented by $L = 228$ samples. The mean RMSE of the simulated perturbation resulted in $3.41 \cdot 10^{-4}$. Utilizing Algorithm 1 with $M = 273$ samples results in mean $Q(\mathbf{e}_p) = 3.23 \cdot 10^{-5}$ which is ≈ 9 times smaller. Calibration performed by taking $M < L$ (Fig. 6(b)) reduces the RMSE to $8.77 \cdot 10^{-5}$, which on average is 3.9 times smaller than the mean error of the initial perturbations.

We also evaluated the reconstruction quality under different error sizes using Algorithms 2 and 3. The results of the reconstruction with and without calibration are presented in Table II. The table columns show the minimum (1), average (2), and maximum (3) recorded error, respectively, within 3000 simulated cases and corresponding SNR values for each error.

TABLE II
IMPULSE RESPONSE RMSE AND CORRESPONDING RECONSTRUCTED SIGNAL SNR (CHEBYSHEV FILTER).

	non-calibrated			calibrated with $M_q = 273$		
	case number			case number		
	1	2	3	1	2	3
RMSE $\cdot 10^4$	0.10	2.93	12.11	0.22	0.26	0.19
SNR dB	68.0	38.3	25.9	75.9	75.1	78.2

We have investigated the performance of (27) with respect to the amount of samples used in the least-squares estimation. Using the Butterworth approximated filter architecture,

we modeled the impulse response with $L = 108$ and performed 11 calibration schemes (27) with different $M_q \in \{42, 63, 105, 126, 189, 315, 630, 1050, 2100, 4200, 8400\}$. The results are shown in Figure 7. The tests utilized calibrating signals with $K \in \{5, 10, 50\}$ tones. Table III juxtaposes the calibration performance in terms of computation time and RMSE. The initial error size in the impulse response was $56.57 \cdot 10^{-5}$.

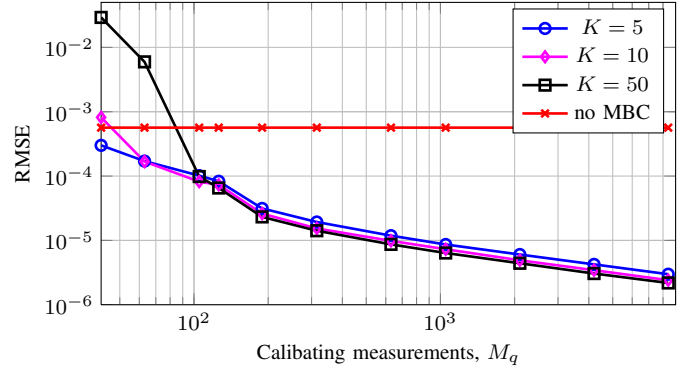


Fig. 7. Calibration performance of the impulse response in RMSE versus the amount of samples used in the least-square estimation (27)

TABLE III
RMSE OF THE CALIBRATED IMPULSE RESPONSE AND THE ACTUAL ONE.

	K	M_q samples					
		42	63	105	126	1050	8400
RMSE $\cdot 10^5$	5	30.02	17.08	10.15	8.30	1.93	0.30
	10	81.73	16.80	8.19	7.30	0.73	0.24
	50	2919.01	595.22	9.83	6.52	1.41	0.22
time [s]	5	0.45	0.45	0.51	0.07	0.07	3.56
	10	0.45	0.45	0.49	0.07	0.13	3.56
	50	0.46	0.45	0.49	0.07	0.07	3.56

C. Benchmarking

Finally, we benchmarked the MBC against the DFTTI method proposed in [10]. The simulation set-up consisted

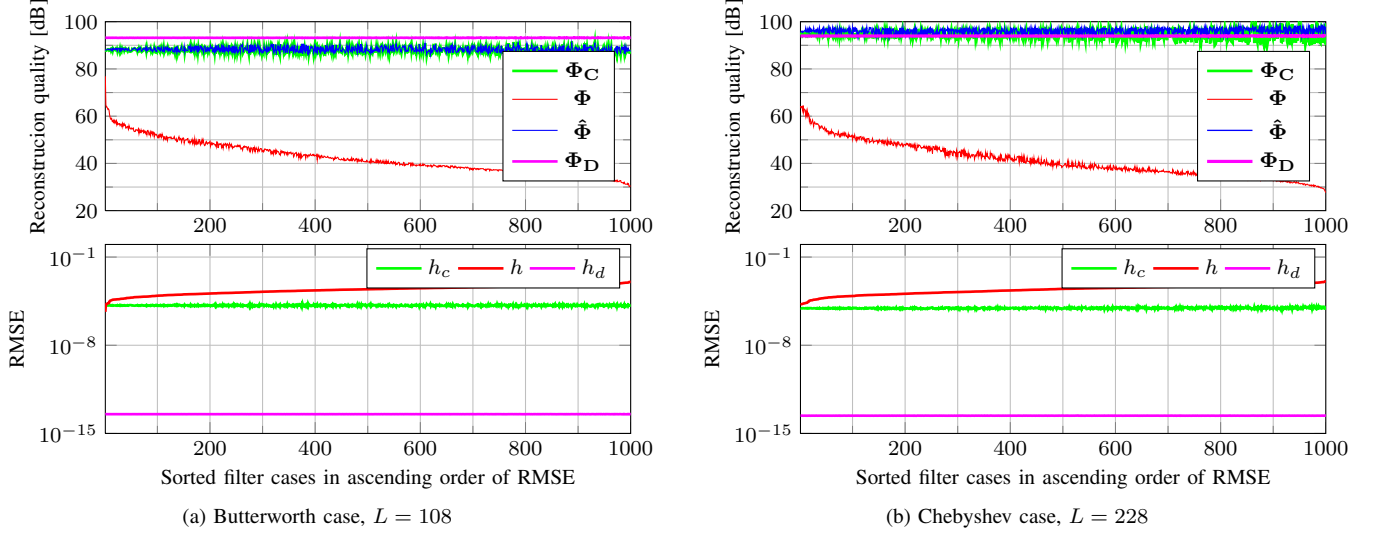


Fig. 8. MBC vs. DFTTI benchmark: $f_N = 12$ kHz, $M_q = 1050$. Four SPGL1 reconstructions were performed with different measurement matrices: Φ_C - calibrated, Φ - ideally modeled, $\hat{\Phi}$ - perturbed (oracle) and Φ_D - DFTTI obtained. RMSE values were calculated between the perturbed (oracle) impulse response and: calibrated h_c , ideally modeled h , and DFTTI obtained h_d .

of the same set of initial parameters as used in previous Monte Carlo simulations. Essentially Algorithms 2 and 3 were utilized to assess the reconstruction quality of each method. Filter realizations (Butterworth and Chebyshev) were subject to component nominal value variation according to (32). We generated 1000 deviating sets of components and sorted the data according to the resulting RMSE. We have recorded SNR, RMSE and the time taken to generate the calibrated measurement matrix Φ_C with model-based calibration or Φ_D using DFTTI. Table IV juxtaposes the results of the benchmark and Fig. 8 visualizes them.

TABLE IV

RMSE, SNR OF THE CALIBRATED IMPULSE RESPONSE AND TIME TAKEN BY THE PROCEDURES: MODEL-BASED CALIBRATION (MBC) AND DFTTI.

Method	RMSE $\cdot 10^7$		SNR [dB]		time [s]	
	DFTTI	MBC	DFTTI	MBC	DFTTI	MBC
Butter.	$3.38 \cdot 10^{-7}$	144.73	93.2	88.0	173.75	0.13
Chebys.	$2.57 \cdot 10^{-7}$	88.91	93.9	94.7	180.98	0.15

The convex solver SPGL1 used to execute the simulations was limited to perform maximum 2500 iterations. This was done to impose a fair reconstruction time limit. The value is sufficiently high to allow perfect reconstruction within the limit, when we solve well-conditioned CS problems ("nice" Φ and $\Phi\Psi$ RIP fulfillment) [3], [16].

D. Discussion

The presented results confirm that the calibration method compensates for filter modeling discrepancies. The method is most reliable in cases of taking a higher amount of samples than the impulse response is represented with ($M_q > L$). We have not observed any problems with the stability of the calibration formulation in (27). On the contrary, when using (29) for $M_q \leq L$, we recorded cases where the RMSE of the

calibrated impulse response $Q(\hat{e}_p) \geq Q(e_p)$. The success rate of the approach downgrades rapidly with decreasing amount of samples and should be considered only when it is infeasible to gather $M_q \geq L$. Also, when taking low amounts of samples, both methods are unable to correct the smallest errors. The data shows that already for $M_q \approx 1.2 \cdot L$, (27) significantly decreases the error in the impulse response, contributing further to the reconstruction quality improvement. Furthermore, the method performance can be tuned by increasing the amount of calibrating signal x_q tones K , as can be seen in Fig. 7. This is related to the condition number of the matrix \mathbf{D} in (25) and modeling density of \mathbf{x} and \mathbf{p} . However, the method in (29) showed performance degradation for increasing K . The method (27) enables sufficient correction of the impulse response but it does not reach the same precision as the DFTTI method. Also, because of the fact that the framework operates on the truncated impulse responses, the reconstruction is more susceptible to component imperfections, which can be observed in Fig. 8. The SNR of the DFTTI method is very stable regardless of the impulse response error. It is important to notice though, that the proposed method requires only an order of M samples to carry out successful calibration as opposed to $M \times N$ used by DFTTI. For the problem of size 800×12600 , DFTTI took 12.6 k samples more than the proposed method, which was the main time-limiting factor. Both of the methods used the same RD signal acquisition framework to facilitate fair time comparison. This makes the model-based calibration method very suitable for systems that require frequent re-calibration.

VI. CONCLUSION

In this article, we presented a supervised model-based calibration method for the random demodulator framework. The calibration addresses the measurement matrix discrepancy that appears when an unaccounted change of the filter

characteristics occurs in the analog front-end of the random demodulator architecture. With the assumption of a known initial filter model, the method exploits the nature of the error and identifies it through linear estimation. The amount of samples necessary to assure successful calibration was orders of magnitude lower when compared to the existing techniques. Through a series of numerical experiments we have shown that the method works independently of the filter realization, and can be used universally as a calibration step before commencing acquisition and reconstruction. The calibration was observed to minimize the error to a level that it was insignificant in affecting the reconstruction quality. This increased the reconstruction of noiseless signal up to 50 dB. The method does not require any modifications to the hardware or its operational frequency, making it easy to implement.

ACKNOWLEDGMENT

The authors would like to thank S. Becker for sharing the DFTTI calibration code utilized in the RMPI framework [10].

REFERENCES

- [1] E. J. Candès, "Compressive sampling," *Proceedings of the International Congress of Mathematicians: Madrid, August 22-30, 2006: invited lectures*, pp. 1433–1452, 2006.
- [2] D. Donoho, "Compressed Sensing," *IEEE Transactions on Information Theory*, vol. 52, no. 4, pp. 1289–1306, 2006.
- [3] E. J. Candès and M. B. Wakin, "An Introduction To Compressive Sampling," *IEEE Signal Processing Magazine*, vol. 25, no. 2, pp. 21–30, 2008.
- [4] S. Kirolos, J. Laska, M. Wakin, M. Duarte, D. Baron, T. Ragheb, Y. Massoud, and R. Baraniuk, "Analog-to-information conversion via random demodulation," *Workshop on Design, Applications, Integration and Software, IEEE Dallas/CAS*, pp. 71–74, 2006.
- [5] J. Laska, S. Kirolos, M. F. Duarte, T. Ragheb, R. G. Baraniuk, and Y. Massoud, "Theory and implementation of an analog-to-information converter using random demodulation," *IEEE International Symposium on Circuits and Systems, ISCAS*, pp. 1959–1962, 2007.
- [6] M. Mishali and Y. C. Eldar, "From theory to practice: Sub-Nyquist sampling of sparse wideband analog signals," *IEEE Journal of Selected Topics in Signal Processing*, vol. 4, no. 2, pp. 375–391, 2010.
- [7] M. Mishali and Y. Eldar, "Xampling: Analog data compression," in *Data Compression Conference (DCC)*, 2010, pp. 366–375.
- [8] T. Ragheb, J. Laska, H. Nejati, S. Kirolos, R. G. Baraniuk, and Y. Massoud, "A prototype hardware for random demodulation based compressive analog-to-digital conversion," *51st Midwest Symposium on Circuits and Systems, MWCAS*, pp. 37–40, 2008.
- [9] D. Yang, H. Li, G. Peterson, and A. Fathy, "Compressed sensing based UWB receiver: Hardware compressing and FPGA reconstruction," in *43rd Annual Conference on Information Sciences and Systems, CISS*, 2009, pp. 198–201.
- [10] S. R. Becker, "Practical compressed sensing : modern data acquisition and signal processing," Thesis (Dissertation (Ph.D.)), California Institute of Technology, Jun. 2011. [Online]. Available: <http://resolver.caltech.edu/CaltechTHESIS:06022011-152525054>
- [11] M. Unser, "Sampling-50 years after Shannon," *Proceedings of the IEEE*, vol. 88, no. 4, pp. 569–587, 2000.
- [12] C. Shannon, "Communication in the presence of noise," *Proceedings of the IRE*, vol. 37, no. 1, pp. 10–21, Jan. 1949.
- [13] J. Tropp and S. Wright, "Computational methods for sparse solution of linear inverse problems," *Proceedings of the IEEE*, vol. 98, no. 6, pp. 948–958, Jun. 2010.
- [14] J. A. Tropp, J. N. Laska, M. F. Duarte, J. K. Romberg, and R. G. Baraniuk, "Beyond Nyquist: Efficient Sampling of Sparse Bandlimited Signals," *IEEE Transactions on Information Theory*, vol. 56, no. 1, pp. 520–544, 2010.
- [15] T. P. Boufounos and M. S. Asif, "Compressive Sensing for streaming signals using the Streaming Greedy Pursuit," 2010, pp. 1205–1210.
- [16] Y. C. Eldar and G. Kutyniok, *Compressed Sensing: Theory and Applications*. Cambridge University Press, 2012.
- [17] P. J. Pankiewicz, T. Arildsen, and T. Larsen, "Sensitivity of the Random Demodulation Framework to Filter Tolerances," in *Proceedings of the European Signal Processing Conference (EUSIPCO)*, 2011, pp. 534–538.
- [18] R. Gribonval, G. Chardon, and L. Daudet, "Blind calibration for compressed sensing by convex optimization," in *IEEE International Conference on Acoustics, Speech and Signal Processing (ICASSP)*, March 2012, pp. 2713–2716.
- [19] M. A. Herman and T. Strohmer, "General Deviants: An Analysis of Perturbations in Compressed Sensing," *IEEE Journal of Selected Topics in Signal Processing*, vol. 4, no. 2, pp. 342–349, 2010.
- [20] M. Herman and D. Needell, "Mixed operators in compressed sensing," in *44th Annual Conference on Information Sciences and Systems, CISS*, Mar. 2010, pp. 1–6.
- [21] Q. Wang and Z. Liu, "Sampling Matrix Perturbation Analysis of Subspace Pursuit for Compressive Sensing," in *Information and Automation*. Berlin, Heidelberg: Springer Berlin Heidelberg, 2011, pp. 581–588.
- [22] M. Rosenbaum and A. B. Tsybakov, "Sparse recovery under matrix uncertainty," *The Annals of Statistics*, vol. 38, no. 5, pp. 2620–2651, Oct. 2010.
- [23] H. Zhu, G. Leus, and G. B. Giannakis, "Sparsity-Cognizant Total Least-Squares for Perturbed Compressive Sampling," *IEEE Transactions on Signal Processing*, vol. 59, no. 5, pp. 2002–2016, 2011.
- [24] Y. Liu and Q. Wan, "Anti-measurement matrix uncertainty for robust sparse signal recovery with the mixed l2 and l1 norms constraint," *ArXiv pre-print*, vol. abs/1006.0054, 2010.
- [25] X. Han, H. Zhang, and H. Meng, "TLS-FOCUSS for sparse recovery with perturbed dictionary," in *IEEE International Conference on Acoustics, Speech and Signal Processing (ICASSP)*, 2011, pp. 3952–3955.
- [26] M. E. Davies and T. Blumensath, "Faster & greedier: algorithms for sparse reconstruction of large datasets," *3rd International Symposium on Communications, Control and Signal Processing, ISCCSP*, pp. 774–779, 2008.
- [27] J. A. Tropp and A. Gilbert, "Signal Recovery From Random Measurements Via Orthogonal Matching Pursuit," *IEEE Transactions on Information Theory*, vol. 53, no. 12, pp. 4655–4666, 2007.
- [28] W. Dai and O. Milenkovic, "Subspace Pursuit for Compressive Sensing Signal Reconstruction," *IEEE Transactions on Information Theory*, vol. 55, no. 5, pp. 2230–2249, 2009.
- [29] S. S. Chen, D. L. Donoho, and M. A. Saunders, "Atomic decomposition by basis pursuit," *SIAM Journal on Scientific Computing*, vol. 20, pp. 33–61, 1998.
- [30] L. Huelsman, *Active and Passive Analog Filter Design: An Introduction*, ser. McGraw-Hill series in electrical and computer engineering: Electronics and VLSI circuits. McGraw-Hill, Inc., 1993.
- [31] A. V. Oppenheim, R. W. Schaffer, and J. R. Buck, *Discrete-time signal processing (2nd ed.)*. Upper Saddle River, NJ, USA: Prentice-Hall, Inc., 1999.
- [32] P. Kinget and M. Steyaert, "Impact of transistor mismatch on the speed-accuracy-power trade-off of analog CMOS circuits," in *Proceedings of the IEEE Custom Integrated Circuits Conference*, May 1996, pp. 333–336.
- [33] M. Steyaert, V. Peluso, J. Bastos, P. Kinget, and W. Sansen, "Custom analog low power design: the problem of low voltage and mismatch," in *Proceedings of the IEEE Custom Integrated Circuits Conference*, May 1997, pp. 285–292.
- [34] P. Kinget, "Device mismatch and tradeoffs in the design of analog circuits," *IEEE Journal of Solid-State Circuits*, vol. 40, no. 6, pp. 1212–1224, Jun. 2005.
- [35] I. Filanovsky, "Sensitivity and Selectivity," in *Circuits & Filters Handbook 3e*. Boca Raton, Florida: CRC Press, LLC, Jan. 2012.
- [36] E. J. Candès, J. K. Romberg, and T. Tao, "Stable signal recovery from incomplete and inaccurate measurements," *Communications on Pure and Applied Mathematics*, vol. 59, no. 8, pp. 1207–1223, 2006.
- [37] D. Donoho, M. Elad, and V. Temlyakov, "Stable recovery of sparse overcomplete representations in the presence of noise," *IEEE Transactions on Information Theory*, vol. 52, no. 1, pp. 6–18, 2006.
- [38] J. A. Tropp, "Just relax: convex programming methods for identifying sparse signals in noise," *IEEE Transactions on Information Theory*, vol. 52, no. 3, pp. 1030–1051, 2006.
- [39] A. Tarantola, *Inverse Problem Theory and Methods for Model Parameter Estimation*. Society for Industrial and Applied Mathematics, 2005.
- [40] J. Oakland, *Statistical Process Control*, ser. Quality management / Butterworth Heinemann. Taylor & Francis, 2003.
- [41] E. van den Berg and M. P. Friedlander, "Probing the pareto frontier for basis pursuit solutions," *SIAM Journal on Scientific Computing*, vol. 31, no. 2, pp. 890–912, 2008.